

1 Elucidating the Field Influence on the Energetics of the Methane Steam  
2 Reforming Reaction: A Density Functional Theory Study

3 Fanglin Che,<sup>a</sup> Su Ha,<sup>a</sup> Jean-Sabin McEwen<sup>\*abc</sup>

4 <sup>a</sup>*The Gene and Linda Voiland School of Chemical Engineering and Bioengineering, Washington State  
5 University, WA, 99164*

6 <sup>b</sup>*Department of Physics and Astronomy, Washington State University, WA, 99164*

7 <sup>c</sup>*Department of Chemistry, Washington State University, WA, 99164*

8 **Abstract**

9 To help realize lower operating-temperatures for the highly endothermic Ni-  
10 catalytic methane steam reforming (MSR) process, we focused on elucidating the  
11 influence of an applied electric field on the energetics of the said reaction. Two aspects  
12 were considered in this study: the electric field effects on (i) the adsorption and electronic  
13 properties of the MSR-involved species, and (ii) the overall MSR energy profile. Our  
14 results show that for Ni-based MSR processes, a positive field strengthens the adsorption  
15 of the reactants, promotes product desorption, impedes coke formation, lowers the overall  
16 energy profiles and consequently, reduces the temperature requirements for the overall  
17 MSR-on-Ni reaction. Based on our phase diagram obtained from first principles, we  
18 show that CO can be obtained from the dehydrogenation of COH and CHO at moderate  
19 hydrogen partial pressure values with a negative field, while methanol is formed on the  
20 surface via hydroxyl oxidation of CH<sub>3</sub> at high hydrogen partial pressures and positive  
21 field values. This investigation suggests ways to facilitate the MSR reforming reaction in  
22 the presence of an electric field and also points towards a number of elementary reactions  
23 that need to be considered for establishing microkinetic model studies.

24 **Keywords:** Methane Steam Reforming; Low Operating Temperatures; Electric Fields;  
25 Electrocatalysis; Phase Diagram.

26 

---

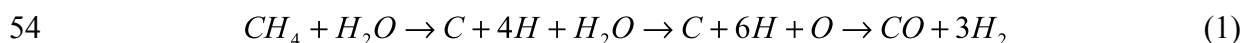
<sup>\*</sup> Corresponding author: Email: [js.mcewen@wsu.edu](mailto:js.mcewen@wsu.edu) (J.-S. McEwen); Phone: (+1)509-335-8580

## 26 **1. Introduction**

27 Hydrogen, the energy carrier of the future, can be used in various applications (e.g.  
28 vehicles and fuel cells) [1] and cater to our dramatically growing need for sustainable  
29 energy resources as well as our ever-present environmental concerns. To generate  
30 hydrogen, steam reforming of natural gas (methane) over Ni-based catalysts is widely  
31 employed in industry [2, 3]. In addition, methane steam reforming (MSR) is a reaction of  
32 interest since it can also be performed directly at the anode of a solid oxide fuel cell  
33 (SOFC) to generate electric power in the direct internal reforming reaction, which  
34 couples steam reforming with subsequent syngas electrochemical oxidation [4-6].  
35 However, the main issue for the said reaction is that methane ( $\text{CH}_4$ ) is very  
36 thermodynamically stable and requires a large amount of energy to break its C-H bonds,  
37 which makes the MSR reaction a highly endothermic process requiring temperatures of  
38 900 K or higher [7]. Consequently, the Ni catalyst is placed in expensive alloy tubes to  
39 tolerate the extremely high thermal fluxes that will occur through the tube walls of the  
40 reactor [8, 9]. An additional problem related to the high operating-temperature  
41 requirements involved in the MSR reaction is the increased occurrence of sintering [10,  
42 11] and coking [12-14], which reduces the lifetime of the Ni catalysts. To rationally  
43 design catalysts with lower temperature requirements for a methane reformer in industrial  
44 or fuel cell applications, it is necessary to understand the thermodynamic properties of the  
45 Ni-based MSR reaction at the atomic scale.

46 The kinetic and thermodynamic properties of methane steam reforming are well  
47 studied [15-19]. Jones et al. showed that the dissociative adsorption of  $\text{CH}_4$  and the  
48 formation of CO are the rate-limiting steps over different transition metals supported by  
49  $\text{Al}_2\text{O}_3$  and  $\text{ZrO}_2$  under MSR conditions from both first principles calculations and

50 experimental investigations [20]. The CO formation barrier is found to be the dominant  
51 rate-limiting step at lower temperatures (773 K), while the dissociative adsorption barrier  
52 for CH<sub>4</sub> is dominant at higher temperatures above 873 K. Bengaard et al. [21] proposed a  
53 possible mechanism over pure Ni catalysts, which is shown in Eq. (1).



55 Their data indicates that C and CH species are the most stable intermediates on Ni(111)  
56 and Ni(211). The overall calculated MSR reaction energy for forming syngas (the total  
57 energy differences between the reactant (CH<sub>4</sub>+H<sub>2</sub>O) and the product (CO+H<sub>2</sub>) in the gas  
58 phase) is 3.03 eV. After correcting the zero-point energies as well as the variation of the  
59 enthalpy of the said reaction at T=298.15 K ( $\Delta C_p \Delta T$ ) [22], the corresponding reaction  
60 enthalpy for the said reaction is 2.38 eV, which is in good agreement with the  
61 experimental value of 2.14 eV. Using DFT calculations, Blaylock's et al. [23] developed  
62 a microkinetic model to investigate the MSR reaction on a Ni(111) surface under realistic  
63 conditions. Similar to Rostrup-Nielsen's work [24], they found that CH is the most  
64 important carbon-containing reaction intermediate. Wang et al. [25]. studied the  
65 stabilities of the intermediates during the CO<sub>2</sub> reforming of CH<sub>4</sub> and found that O, CH<sub>3</sub>,  
66 CH<sub>2</sub>, CH and CHO were key intermediates, in which the most favorable mechanism is for  
67 follows:



69 However, thus far, the influence of the environment on the underlying reaction  
70 mechanism over heterogeneous catalysts is still largely unexplored.

71 One possible route to achieve lower operating-temperature requirements for the  
72 MSR reaction is to study the effects of the electric field on its mechanism [26-28]. Gorin

73 et al. applied interfacial electric fields, generated from a parallel plate cell with a voltage  
74 source, to the  $\text{Al}_2\text{O}_3$  catalytic rearrangement of *cis*-stilbene oxide. The results showed that  
75 the reaction conversion of the *cis*-stilbene oxide to the aldehyde and ketone products  
76 increased up to 10 times higher in the presence of an interfacial electric field as compare  
77 to the one with no electric fields. And the aldehyde to ketone product ratio increased from  
78 1:4 (without electric fields) to 17:1 (in the presence of an electric field) [26]. Sekine et al.  
79 investigated the electric field effects on the methane steam reforming over Pd/CeO<sub>2</sub>,  
80 Ru/CeO<sub>2</sub> and Pt/CeO<sub>2</sub> catalysts, so called “electro-reforming” [27, 28]. The methane  
81 conversion was largely enhanced with an electric field over all catalysts as well as the  
82 hydrogen production yields. Furthermore, our previous work concluded that a positive  
83 field could significantly reduce pure carbon deposits over Ni catalysts by decreasing the  
84 stabilities of pure carbon atoms and increasing the activation energy barrier for CH  
85 dissociation. In addition, the presence of a positive field strengthened the adsorption of  
86 H<sub>2</sub>O, while a negative electric field had an opposite effect. Moreover, we examined  
87 methane and water dissociation over flat and stepped Ni surfaces and found similar  
88 electric field effects on both Ni surfaces for the above-mentioned reactions [29-31].

89         There are several approaches to apply an electric field in the theoretical work,  
90 such as the Neugebauer and Scheffler’s method [32] (NS) and Neurock group’s double  
91 reference method [33, 34]. For the NS approach [32], one inserts a dipole sheet in the  
92 middle of the vacuum of a supercell to polarize the metal surface. The polarization  
93 induces opposite charges on the top and bottom of the metal surfaces and thereby  
94 generates a uniform electric field ( $F$ ) at a given specified value. With this approach, the  
95 interaction between the metal and the adsorbate depends on the effective dipole moment

96 and the effective polarizability of the system. Large electric fields, on the order of  $\pm 1$   
97  $\text{V}/\text{\AA}$ , can rearrange the molecular or atomic orbitals of the intermediates, which can  
98 directly alter the stabilities of the reaction intermediates and consequently change the  
99 underlying reaction mechanism [35-37]. To relate the applied field to the electrode  
100 potential, a rough approximation based on a Helmholtz model proposed by Janik and  
101 coworkers was proposed,[38, 39]:

$$102 \quad F = (U - U(\text{PZC})) / d \quad (3)$$

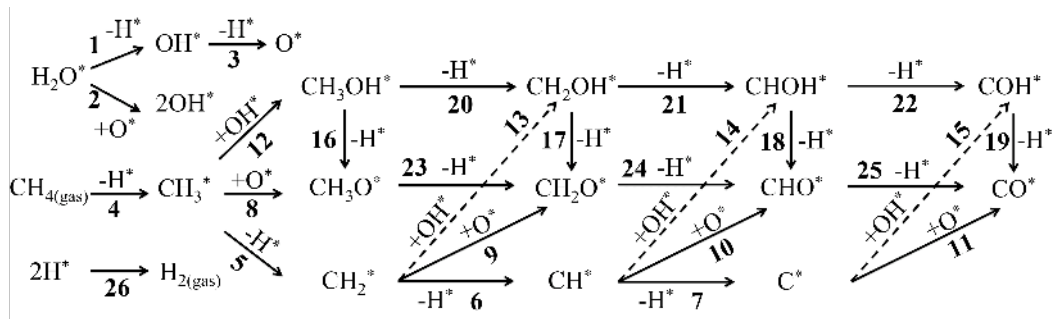
103 where  $d$  is the distance between the electrode surface and counter-ion charge plane (i.e.  
104 the thickness of the Helmholtz layer of a fuel cell system).  $U(\text{PZC})$  is the potential of  
105 zero charge, which varies from one metal surface to another and for different ion  
106 compositions.  $U(\text{PZC})$  is often approximated to be 0 on the reversible hydrogen electrode  
107 (RHE) scale. Therefore, for an electric field of  $0.5 \text{ V}/\text{\AA}$  within a Helmholtz layer of  $3 \text{ \AA}$ ,  
108 the electrode potential is  $1.5 V_{\text{RHE}}$ . However, such an approximation cannot capture the  
109 impact of the adsorbate in shifting the metal work function, which especially needs to be  
110 improved when an adsorbate/electrode system has a large dipole moment. On the other  
111 hand, adjusting the number of electrons within the unit cell and adding a compensating  
112 homogeneous background charge in the double reference method [39] can change the  
113 surface potential and generate an electric field at the electrode-electrolyte interface.[38]  
114 The electric field is related to the electrode potential ( $V_{\text{NHE}}$ ) by:

$$115 \quad V_{\text{NHE}} = \phi / e - 4.6 \quad (4)$$

116 Where  $\phi$  is the calculated work function referenced to vacuum,  $e$  is the charge of an  
117 electron and  $4.6 \text{ V}$  is the estimated potential of the vacuum of the NHE scale in fuel  
118 cells.[40] In addition, to generate electrode potentials above  $1.1 \text{ V}$  (or below  $0.5 \text{ V}$ ), the

119 top of the metal slab is positively charged (or negative charged) by selectively adding  
 120 (subtracting) a number of electrons to the system. This corresponds with the calculated  
 121 system in the presence of a simulated positive field (a simulated negative field) in the NS  
 122 method since such a system includes a positively charged (a negatively charged) metal  
 123 slab.

124 In this present paper, by using the NS method, we will show the significance of  
 125 the electric field effects on the energetics of the MSR-on-Ni reaction. Several researchers  
 126 have proposed [41-43] that surface OH and O species can be key intermediates that react  
 127 with the surface  $\text{CH}_x$  species. Thus we examined mechanisms for the overall MSR  
 128 reaction that include both  $\text{CH}_x\text{OH}$  and  $\text{CH}_x\text{O}$  species (given in Fig. 1). To identify the  
 129 relative equilibrium stabilities of the MSR intermediates under realistic conditions, we  
 130 also provide a first-principles-based phase diagram for the  $\text{CH}_x\text{OH}$  and  $\text{CH}_x\text{O}$  species as  
 131 a function of the hydrogen chemical potential and the applied electric field. Based on our  
 132 previous studies, we also anticipate that many of the results obtained here on a Ni(111)  
 133 flat surface will be applicable to stepped surfaces as well [29-31]. The paper ends with  
 134 the significant findings on the field effects on the heterogeneous reaction and an outlook  
 135 on the remaining challenges of field-dependent heterogeneous reactions.



136

137 **Fig. 1.** Proposed mechanisms of methane steam reforming (MSR) on Ni(111).

138 **2. Methods**

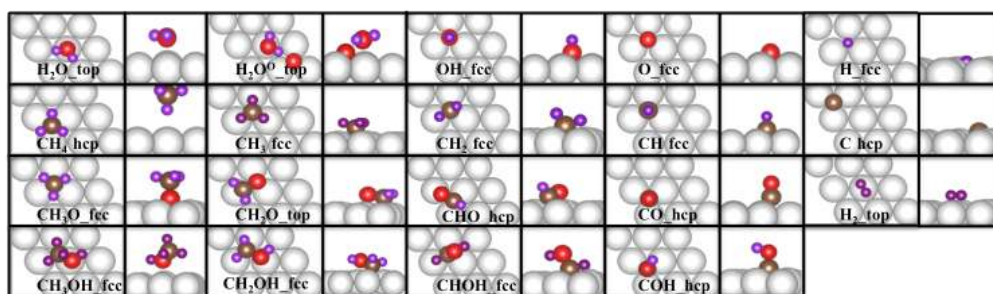
139 Our DFT calculations were performed with the Vienna *Ab Initio* Simulation  
140 Package (VASP). For adsorbates/late transition metal system, it was recently found in a  
141 benchmarking study that the Perdew-Wang 91 functional is of comparable accuracy to  
142 the PBE, PBEsol and RPBE functionals when examining a large variety of adsorption  
143 systems [44]. As a result, for all calculations we used the Generalized Gradient  
144 Approximation with the PW91 exchange correlation functional (GGA-PW91) [45-47].  
145 The projector-augmented wave method was applied to solve the Kohn-Sham equations  
146 [48]. The choices for the k-point mesh ( $4 \times 4 \times 1$ ), the lattice constant of Ni (3.521 Å),  
147 the plane-wave energy cutoff (400 eV), the vacuum size (11 Å) [31, 49], and four-layer  
148 Ni slab was tested in our previous work [29-31]. An increase in the energy cutoff to 450  
149 eV and the  $k$ -point mesh to  $6 \times 6 \times 1$  kpoints was found to change the adsorption energies  
150 of  $\text{CH}_x$  by less than 0.02 eV [29]. The adsorption energies differences between our 4-  
151 layer and 5-layer Ni slab models were all less than 0.01 eV [31]. Therefore, all the  
152 energies reported in this manuscript are estimated with an accuracy of 0.01 eV.  
153 Additionally, we considered the influence of van der Waals corrections (optB88-vdW) on  
154 the physisorption of a  $\text{CH}_4$  molecule over a Ni(111) surface in the presence of the electric  
155 field. The inclusion of the van der Waals forces strengthened the adsorption energy  
156 methane by  $\sim 0.13$  eV and shifted the dissociation of methane to form  $\text{CH}_3$  and H by only  
157  $\sim 0.02$  eV regardless of the electric field strength (see Fig. S10). Since these changes are  
158 not significant, we used PW91 functional in our DFT calculations.

159 Adsorption energies ( $E_{\text{ad}}$ ) of isolated intermediates on a Ni(111) surface were  
160 calculated from Eq. (5) and the reaction energies ( $\Delta H_{\text{rxn}}$ ) of the  $A + B \rightarrow C + D$   
161 elementary reactions were calculated by Eq. (6):

162 
$$E_{ad} = E_{A/sl\text{ab}} - E_{sl\text{ab}} - E_A \quad (5)$$

163 
$$\Delta H_{rxn} = E_{C+D/sl\text{ab}} - E_{A+B/sl\text{ab}} \quad (6)$$

164 where  $E_{A/sl\text{ab}}$ ,  $E_{sl\text{ab}}$ , and  $E_A$  are the total energies of molecule **A** adsorbed on the slab, the  
 165 clean slab, gas phase molecule **A**, respectively. Endothermic reactions are accompanied  
 166 by positive values of  $\Delta H_{rxn}$ .



167  
 168 **Fig. 2.** The top and side views of the most favorable adsorption structures of all MSR-involved  
 169 possible intermediates on a Ni(111) surface. For the  $\text{CH}_x\text{OH}_y$  species, the site labeling refers to  
 170 the surface carbon position.

### 171 3. Results and Discussion

#### 172 3.1. Electric field effects on the adsorption energy of MSR intermediates

173 To better understand the field effects on the MSR reaction, we simulate the  
 174 influence of an electric field on the order of  $-1 \text{ V/\AA}$  to  $1 \text{ V/\AA}$  on this system. With such  
 175 strong applied electric field, the metal/adsorbate system interacts with a field that can  
 176 stabilize or destabilize the adsorbate based on both the surface dipole moment as well as  
 177 the polarizability it induces to the interface, and subsequently alter the mechanisms of the  
 178 heterogeneous reactions. The field effects on the adsorption energies ( $E_{ad}$ ) of the MSR  
 179 species at their most favorable configurations (Fig. 2) are given in Table 1 and Fig. 3.  
 180 The electronic structures with tunable electric fields for  $\text{H}_2\text{O}$ , OH, O and  $\text{CH}_x$  ( $x=0\sim 3$ )  
 181 species have been already discussed in our previous work [29, 31]. The details regarding



182 to the adsorption structures of various MSR-involved species over Ni(111) in the absence  
 183 of an electric field are given in the ESI Section 1.

184 **Table 1.** Summary of electric field effects on the adsorption of possible MSR intermediates at  
 185 their most favorable adsorption sites.

Species	Site	$E_{ad}$ (eV)	$d_{C(O)-H}$ (Å)	$d_{C-O}$ (Å)	$d_{Ni-O(C)}$ (Å)
CH <sub>4</sub>	hcp	-0.00 / -0.04 / -0.09	1.10 / 1.10 / 1.10	---	4.06 / 4.05 / 4.04
CH <sub>3</sub> O	fcc	-2.94 / -2.84 / -2.67	1.10 / 1.10 / 1.10	1.42 / 1.44 / 1.46	1.99 / 1.98 / 1.96
CH <sub>2</sub> O	top	-0.45 / -0.80 / -1.11	1.10 / 1.10 / 1.10	1.39 / 1.38 / 1.37	2.01 / 1.99 / 1.98
CHO	hcp	-2.28 / -2.35 / -2.05	1.11 / 1.11 / 1.11	1.30 / 1.29 / 1.28	1.95 / 1.96 / 1.97
CO	hcp	-2.11 / -1.93 / -1.69	---	1.21 / 1.19 / 1.18	1.94 / 1.95 / 1.96
CH <sub>3</sub> OH	fcc	-0.05 / -0.31 / -0.47	1.10 / 1.10 / 1.10	1.43 / 1.45 / 1.46	4.02 / 2.15 / 2.08
CH <sub>2</sub> OH	fcc	-1.12 / -1.70 / -1.34	1.11 / 1.10 / 1.12	1.45 / 1.46 / 1.45	2.43 / 2.14 / 2.07
CHOH	fcc	-3.29 / -3.05 / -2.74	1.16 / 1.18 / 1.21	1.40 / 1.37 / 1.35	1.97 / 1.96 / 1.96
COH	hcp	-4.54 / -4.53 / -4.19	0.98 / 0.98 / 0.99	1.37 / 1.34 / 1.31	1.85 / 1.86 / 1.87
H <sub>2</sub>	top	-0.14 / -0.27 / -0.38	---	---	---

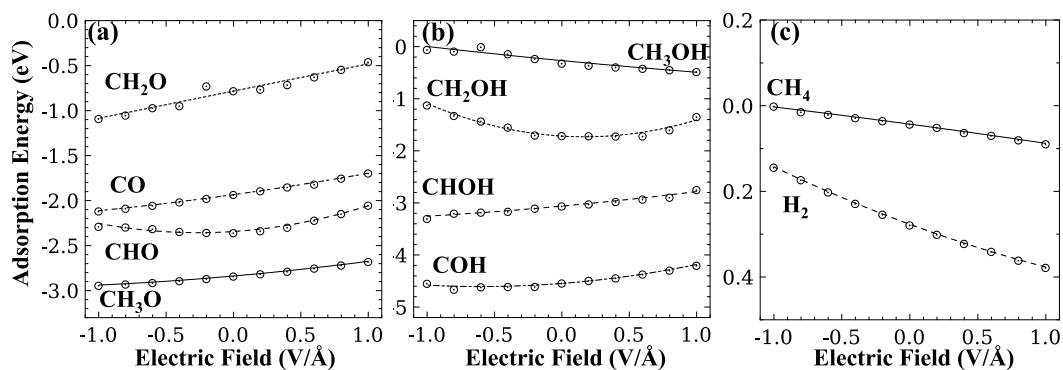
186 Note: The numbers in each column from left to right represent the adsorption of possible intermediates in  
 187 the presence of a negative electric field, in the absence of an electric field, and for a positive electric field  
 188 value, respectively. For the  $d_{C(O)-H}$  column, we only measured O-H distance for a COH molecule, while the  
 189 others represent the C-H distance. For the  $d_{Ni-O(C)}$  column, we measured Ni-O distance for CH<sub>3</sub>O, CH<sub>2</sub>O,  
 190 CH<sub>3</sub>OH molecules, while the others represent the Ni-C distance.

191

### 192 3.1.1 Electric field effects on the adsorption of CH<sub>x</sub>O species

193 Fig. 3(a) shows the adsorption energies of the most favorable CH<sub>x</sub>O (x=0~3)  
 194 configurations as a function of the applied electric field strength. Applied electric fields  
 195 affect the adsorption energies of CH<sub>3</sub>O, CH<sub>2</sub>O and CO in a similar way, in which their  
 196 adsorption energies are monotonically weakened as the field strength is increased from -1  
 197 V/Å to 1 V/Å. In contrast to the other CH<sub>x</sub>O species, both positive and negative fields  
 198 decrease the adsorption strength of CHO. Comparing the field effects on all of the CH<sub>x</sub>O  
 199 species, we find that the CH<sub>2</sub>O species has the largest influence: the adsorption energy of  
 200 CH<sub>2</sub>O differs by up to 0.6 eV for field values ranging from -1 V/Å to 1 V/Å. Since the  
 201  $E_{ad}$  value of a CH<sub>2</sub>O molecule is only -0.45 eV in the presence of a positive field of 1

202  $\text{V}/\text{\AA}$ ,  $\text{CH}_2\text{O}$  likely desorbs from the surface as a byproduct rather than adsorbing as a  
 203 MSR reaction intermediate. Importantly, since the adsorption energy of CO is  $\sim 0.5$  eV  
 204 smaller at a field value of  $1 \text{ V}/\text{\AA}$  as compared to when a field strength of  $-1 \text{ V}/\text{\AA}$  is  
 205 applied, we also conclude that a strong positive electric field can assist in the desorption  
 206 of the CO product from a flat Ni surface.

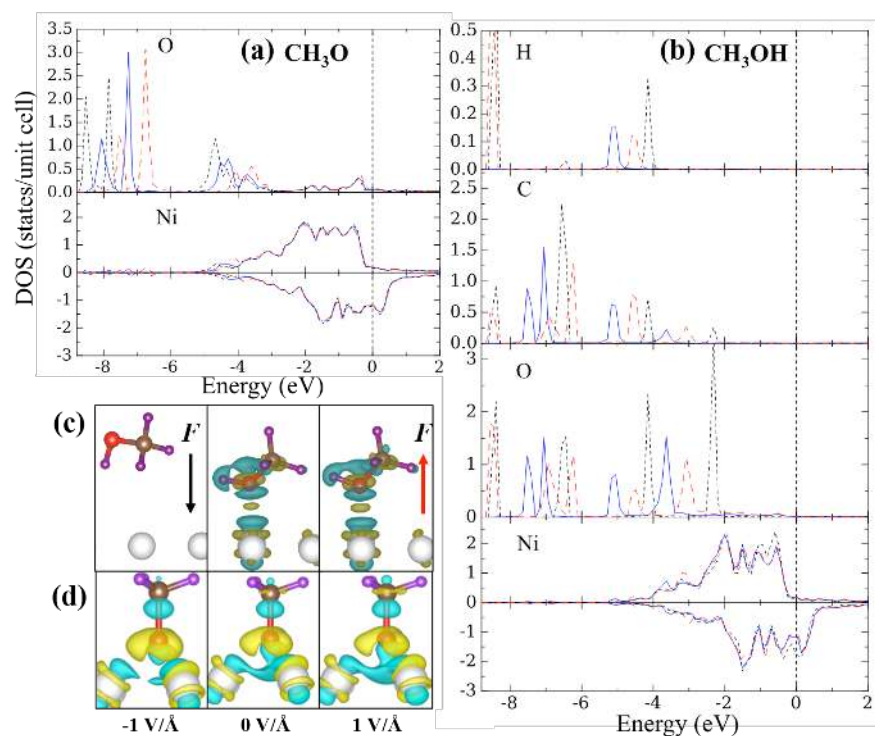


207

208 **Fig. 3.** The field-dependent trendlines of the MSR-involved species as the function of an applied  
 209 electric field, including the (a)  $\text{CH}_x\text{O}$  species ( $x=0\sim 3$ ), the (b)  $\text{CH}_x\text{OH}$  species ( $x=0\sim 3$ ) and the (c)  
 210  $\text{CH}_4$  and  $\text{H}_2$  species. The dots represent their adsorption energies under a particular electric field  
 211 strength ranging from  $-1 \text{ V}/\text{\AA}$  to  $1 \text{ V}/\text{\AA}$  at an interval of  $0.2 \text{ V}/\text{\AA}$ .

### 212 3.1.2 Electric field effects on the adsorption of the $\text{CH}_x\text{OH}$ species

213 The electric field effects on the adsorption of the  $\text{CH}_x\text{OH}$  ( $x=0\sim 3$ ) species on  
 214 Ni(111) are shown in Fig. 3(b). The field effects on the adsorption of  $\text{CH}_2\text{OH}$  and  
 215  $\text{CH}_3\text{OH}$  are similar to the ones of  $\text{H}_2\text{O}$  on Ni(111) from our previous work [31], the  
 216 adsorption energies of  $\text{CH}_3\text{OH}$  strengthen from  $-0.05$  eV to  $-0.47$  eV and the adsorption  
 217 geometries of the OH segment of  $\text{CH}_3\text{OH}$  alters from a H-down structure to H-up  
 218 structure as we increase the fields from  $-1 \text{ V}/\text{\AA}$  to  $1 \text{ V}/\text{\AA}$  (Fig. 4).



219

220 **Fig. 4.** Projected density of state (DOS) of of CH<sub>3</sub>O (a) and CH<sub>3</sub>OH (b) on the Ni(111) surface  
 221 and parts (c) and (d) present their differential charge densities in the presence and the absence of  
 222 an electric field. Red, blue and black lines in part (a) and (b) represent the DOS with a positive  
 223 field, no fields and a negative field, respectively. The energy scale of the DOS are relative to the  
 224 Fermi energy, as indicated by the vertical black dotted line. The isosurface level of the  
 225 differential charge densities of CH<sub>3</sub>O (c) and CH<sub>3</sub>OH (d) are 0.003 and 0.007 e/bohr<sup>3</sup>. The yellow  
 226 or blue areas represent a gain or loss of electrons.

### 227 3.1.3 Electric field effects on the adsorption of MSR-involved species

228 In combination with our previous work [29, 31] along with the results in the  
 229 present investigation on the adsorption of the CH<sub>x</sub> (x=0~3) and the H<sub>x</sub>O (x=0~2) species  
 230 as a function of the electric field strength, we conclude several key points here. A  
 231 positive electric field strengthens the adsorption of reactants (CH<sub>4</sub> + H<sub>2</sub>O) on Ni(111) and  
 232 facilitates the desorption of products (CO+H<sub>2</sub>). The electric field effects on the adsorption  
 233 energies of CH<sub>x</sub>O and CH<sub>x</sub>OH are more significant than those on the CH<sub>x</sub> species [29].

234 Interestingly, the chemisorption species, such like  $\text{CH}_3\text{O}$ ,  $\text{CHO}$ ,  $\text{CHOH}$  or  $\text{COH}$ , have  
235 similar dependence on the electric field, in which a negative electric field further  
236 stabilizes their adsorption. Conversely, the physisorbed byproducts, such as  $\text{CH}_3\text{OH}$ ,  
237  $\text{CH}_2\text{O}$  are further destabilized on the surface with a negative electric field. However, such  
238 an influence of an electric field on the adsorption of methanol is also of interest since it is  
239 a more desirable product than syngas for other industrial applications [50].

### 240 3.2. Electronic properties analysis for electric field effects

#### 241 3.2.1 Adsorption geometries

242 Table 1 shows how an electric field, on the order of  $-1 \text{ V/\AA}$  to  $1 \text{ V/\AA}$ , influences  
243 the adsorption geometries of MSR intermediates on a Ni(111) surface. In comparison  
244 with the geometries in the absence of a field, the O atoms of all  $\text{CH}_x\text{OH}$  ( $x=0\sim 3$ ) and  
245  $\text{CH}_x\text{O}$  ( $x=0\sim 3$ ) species are farther away from the surface when a negative electric field is  
246 applied, while the O atoms of these species are closer towards the surface when applying  
247 a positive electric field. This is similar to our previous work on the electric field effects  
248 on the adsorption geometries of  $\text{H}_2\text{O}$  on Ni(111) [31]. The reason for these effects is that  
249 the O atoms of all  $\text{CH}_x\text{OH}$  ( $x=0\sim 3$ ) and  $\text{CH}_x\text{O}$  ( $x=0\sim 3$ ) species are negatively charged,  
250 which is attracted to the positively charged metal surface in the presence of a positive  
251 electric field. On the other hand, a negative electric field direction points towards the  
252 surface (as shown in Fig. 4) and polarizes the top of the Ni surface with a partial negative  
253 charge and consequently repels the negatively charged O atoms. This explanation also  
254 can be used to better understand the adsorption of the  $\text{CH}_x$  species when the C atom is  
255 bonded to the surface. For example, the C atom of a  $\text{CH}_4$  molecule is partially negatively  
256 charged. As a result, the C atom is closer to the surface when a positive electric field is  
257 applied and is further away from the surface when we apply a negative electric field.

258 Conversely, the C atom in a CO and a COH molecule is partially positively charged and  
259 an electric field has the opposite effect on the Ni-C distance as compared to its effect on  
260 the Ni-C distance on a CH<sub>x</sub> molecule.

### 261 3.2.2 Effective dipole moments and effective polarizability analysis

262 The effect of a simulated field on the  $E_{ad}$  values of the species involved in the  
263 MSR reaction can be given in terms of a Taylor series expansion [33, 34, 51-55]:

$$264 \quad E_{ad} = E_{ad0} - \Delta d_{F=0} F - \frac{1}{2} \Delta \alpha_{F=0} F^2 + \dots \quad (5)$$

265 where all the Taylor coefficients,  $E_{ad0}$ ,  $\Delta d_{F=0}$  (effective dipole moment), and  $\Delta \alpha_{F=0}$   
266 (effective polarizability [53]) are evaluated at  $F = 0$  V/Å. More details on how to derive  
267 this equation can be found in our previous work [31]. The values of  $\Delta d_{F=0}$  and  $\Delta \alpha_{F=0}$  of  
268 all MSR-involved species are the first and second derivatives of field-dependent energies  
269 (Fig. 3), which are summarized in Table 2.

270 From Fig. 3, it is clear that the adsorption of CH<sub>2</sub>O has the most significant field  
271 effect, which correlates well with the fact that its effective dipole moment in Table 2 is  
272 the largest. Fig. 3(a) shows that the CH<sub>3</sub>O, CH<sub>2</sub>O and CO species have similar electric  
273 field effect trends. A positive electric field weakens their adsorption energies and a  
274 negative electric field strengthens them. This also correlates well with the fact that the  
275 signs of their effective dipole moments are all positive. The sign of the dipole moments  
276 of all weakly adsorbed species (CH<sub>3</sub>OH, CH<sub>4</sub>, H<sub>2</sub>O and H<sub>2</sub>) are the same as well, and thus  
277 the field has similar influences on the weakly adsorbed species. Therefore, we conclude  
278 that the field influence on the adsorption energy mainly depends on the magnitude of

279 their corresponding effective dipole moments. We also find that the magnitude of  $\Delta d_{F=0}$   
 280 for all the MSR-involved species obeys the following order:  $CH_xO > CH_xOH > H_xO > CH_x$ .  
 281 **Table 2.** Summary of the effective dipole moments (in units of  $eV \cdot \text{\AA}/V$ ) and effective  
 282 polarizabilities (in units of  $eV \cdot \text{\AA}^2/V^2$ ) for the MSR-involved species on Ni(111).

IS	$\Delta d_{F=0}$	$\Delta \alpha_{F=0}$	FS	$\Delta d_{F=0}$	$\Delta \alpha_{F=0}$
<b>H<sub>2</sub>O</b>	<b>0.25</b>	<b>-0.15</b>	OH, H	0.08	-0.52
<b>OH</b>	-0.09	-0.05	<b>O, H</b>	<b>-0.34</b>	<b>-0.06</b>
<b>O</b>	-0.08	-0.20			
<b>H<sub>2</sub>O, O</b>	0.21	-0.40	OH, OH	-0.13	0.19
<b>CH<sub>4</sub></b>	0.04	0.00	<b>CH<sub>3</sub>, H</b>	<b>0.14</b>	<b>-0.09</b>
<b>CH<sub>3</sub></b>	<b>0.19</b>	<b>-0.02</b>	CH <sub>2</sub> , H	-0.06	-0.02
<b>CH<sub>2</sub></b>	0.14	-0.02	CH, H	-0.07	-0.01
<b>CH</b>	0.08	-0.19	C, H	-0.15	-0.05
<b>C</b>	-0.07	-0.18			
<b>CH<sub>3</sub>O</b>	-0.13	-0.06	<b>CH<sub>3</sub>, O</b>	<b>0.19</b>	<b>-0.11</b>
<b>CH<sub>2</sub>O</b>	<b>0.30</b>	<b>0.00</b>	CH <sub>2</sub> O, H	-0.18	-0.06
<b>CHO</b>	-0.10	-0.38	CH <sub>2</sub> , O	-0.04	0.05
<b>CO</b>	-0.21	-0.06	CHO, H	-0.09	-0.02
			CH, O	-0.01	0.06
			<b>CO, H</b>	<b>-0.22</b>	<b>-0.01</b>
			C, O	-0.04	0.09
<b>CH<sub>3</sub>OH</b>	<b>0.25</b>	<b>-0.05</b>	CH <sub>3</sub> , OH	-0.13	0.52
			CH <sub>2</sub> OH, H	-0.03	-0.41
			CH <sub>3</sub> O, H	0.02	-0.24
<b>CH<sub>2</sub>OH</b>	0.16	-0.93	CH <sub>2</sub> , OH	0.12	-0.07
			<b>CHOH, H</b>	<b>-0.17</b>	<b>-0.03</b>
			<b>CH<sub>2</sub>O, H</b>	<b>-0.14</b>	<b>-0.07</b>
<b>CHOH</b>	-0.24	-0.08	<b>CH, OH</b>	<b>0.23</b>	<b>-0.09</b>
			COH, H	0.11	-0.02
			CHO, H	-0.06	-0.08
<b>COH</b>	-0.20	-0.33	C, OH	-0.01	0.14
			<b>CO, H</b>	<b>-0.37</b>	<b>-0.11</b>
<b>H</b>	-0.01	-0.03	H, H	0.14	0.04
<b>H<sub>2</sub></b>	0.12	-0.07			

283 Note: 'H<sub>2</sub>O, O' represents the adsorption of a H<sub>2</sub>O molecule with a pre-adsorbed O atom

### 284 3.2.3 Electronic properties analysis

285 In Section 3.1 and 3.2.2, we found that the presence of an electric field gave  
 286 similar trends for the strongly adsorbed species (e.g. CH<sub>3</sub>O) and had opposite trends for  
 287 the weakly adsorbed species (e.g. CH<sub>3</sub>OH). To give a qualitative analysis on the electric  
 288 field effects on the electronic interactions between the adsorbates and the metal surface,  
 289 we present both the project density of states (PDOS) and a differential charge density

290 analysis of the isolated adsorbed MSR intermediates ( $\text{CH}_x\text{O}$  and  $\text{CH}_x\text{OH}$  groups) on the  
291 Ni(111) surface. Since the electronic properties of the strongly adsorbed species ( $\text{CH}_2\text{O}$ ,  
292  $\text{CHO}$ ,  $\text{CO}$ ,  $\text{CHOH}$  and  $\text{COH}$ ) are similar to  $\text{CH}_3\text{O}$  and the weaker adsorbed species  
293 ( $\text{CH}_2\text{OH}$ ) have similar trends as that found for  $\text{CH}_3\text{OH}$ , we only show the DOS and  
294 differential charge density analysis of  $\text{CH}_3\text{O}$  and  $\text{CH}_3\text{OH}$  in Fig. 4. More details  
295 regarding to the DOS and the differential charge density analysis of the other  $\text{CH}_x\text{O}$  and  
296  $\text{CH}_x\text{OH}$  species are given in Fig. S11-S13. Furthermore, the differential charge density  
297 shows that an adsorbed  $\text{CH}_3\text{OH}$  molecule has no charge transfer with the metal surface in  
298 the presence of a negative field but has a significant amount of charge transfer for  
299 positive field values, which corresponds well with the monotonically increasing  
300 adsorption energy of  $\text{CH}_3\text{OH}$  with increasing field strength. Similarly, the O atom gains  
301 slightly more electrons from the metal surface when examining the differential charge  
302 density of  $\text{CH}_3\text{O}$  in the presence of a negative field than it does in the presence of a  
303 positive field or in the absence of a field. This also correlates well with its adsorption  
304 energy since it is stronger for negative field values than it is in the absence of a field or  
305 for positive field strengths.

#### 306 3.2.4 Bader charge analysis

307 To give a quantitative analysis on the electric field effects on the charge transfer  
308 at the interface of the adsorbate/metal system, we present in Table 3 a Bader charge  
309 summary [56]. When we calculated the Bader charge analysis, we applied a fast Fourier  
310 transform (FFT) grid that was twice as dense as compared to the standard FFT grid so as  
311 to ensure that the Bader charge results were fully converged. In Table 3,

312

313 **Table 3.** Bader charge analysis of the MSR intermediates as a function of an electric  
 314 field.

Species	$\Delta e = \text{Ni}(e) - 360e$	$\Delta e = \text{O}(e) - 6e$	$\Delta e = \text{C}(e) - 4e$	$\Delta e = \text{nH}(e) - ne$
<b>CH<sub>4</sub></b>	-0.05 / -0.02 / 0.01	---	0.17 / 0.13 / 0.13	-0.12 / -0.11 / -0.14
<b>CH<sub>3</sub>O</b>	-0.59 / -0.50 / -0.41	1.09 / 1.06 / 1.03	-0.41 / -0.35 / -0.30	-0.09 / -0.22 / -0.32
<b>CH<sub>2</sub>O</b>	-0.62 / -0.49 / -0.36	1.01 / 0.99 / 0.97	-0.30 / -0.32 / -0.33	-0.09 / -0.18 / -0.28
<b>CHO</b>	-0.55 / -0.43 / -0.31	1.04 / 0.99 / 0.95	-0.41 / -0.43 / -0.45	-0.07 / -0.13 / -0.20
<b>CO</b>	-0.49 / -0.38 / -0.28	1.07 / 1.02 / 0.96	-0.58 / -0.64 / -0.68	---
<b>CH<sub>3</sub>OH</b>	-0.07 / 0.00 / 0.08	1.14 / 1.13 / 1.12	-0.39 / -0.31 / -0.29	-0.68 / -0.82 / -0.91
<b>CH<sub>2</sub>OH</b>	-0.34 / -0.23 / -0.13	1.12 / 1.07 / 1.06	-0.08 / -0.04 / -0.04	-0.71 / -0.80 / -0.89
<b>CHOH</b>	-0.34 / -0.24 / -0.11	1.05 / 1.07 / 1.17	-0.22 / -0.20 / -0.27	-0.60 / -0.63 / -0.68
<b>COH</b>	-0.39 / -0.27 / -0.15	1.14 / 1.10 / 1.13	-0.15 / -0.21 / -0.31	-0.60 / -0.62 / -0.67
<b>H<sub>2</sub></b>	-0.07 / -0.02 / 0.04	---	---	0.07 / 0.02 / -0.04

315 Note: 1. The number in each column from left to right represents the charge differences of the species in  
 316 the presence of a negative electric field, in the absence of a field, and a positive electric field, respectively.

317 2. The 2<sup>nd</sup> column ' $\Delta e = \text{Ni}(e) - 360e$ ' represents the charge gain or loss of the metal surface for each  
 318 intermediate since each Ni atom has 10 e and we have 36 Ni atoms in each metal slab. This number also  
 319 equals the charge loss or gain of the corresponding adsorbates.

320 3. The 3<sup>rd</sup>, 4<sup>th</sup> and 5<sup>th</sup> column show the charge gain or loss for the O, C and H atoms in each species.

321 4. A positive sign means that the system gains a charge, while the negative sign stands for a charge loss.

322

323 In the absence of a field, the CH<sub>3</sub>OH, CH<sub>4</sub>, and H<sub>2</sub> have almost no electronic  
 324 interactions with the metal surface. This correlates well with the fact that these species  
 325 adsorb very weakly on the Ni surface. These weakly adsorbed species have similar field  
 326 effects on their charges. With a positive electric field, the adsorbates gain slightly more  
 327 charges from the surface than the scenarios in which there are no fields, which correlates  
 328 well with the fact that a positive field only alters their adsorption strength slightly. For  
 329 negative field values, the surface becomes partially negatively charged and this repels the  
 330 negatively charged C atom of the adsorbed species (e.g. CH<sub>3</sub>OH, CH<sub>4</sub>) and consequently  
 331 leads to a much weaker adsorption.

332 Similar electric field effects are found for the other MSR intermediates, including  
 333 CH<sub>x</sub>O (x=0~3) and CH<sub>x</sub>OH (x=0~2). In the absence of a field, the O atoms of the above  
 334 species gain ~1 e from both the metal slab and the CH<sub>x</sub> segment, and become negatively



335 charged. The H atom, which is bonded to the O atom of  $\text{CH}_x\text{OH}$  species, loses  $\sim 0.85 e$   
336 and becomes positively charged. Overall, these intermediates gain a net charge from the  
337 Ni surface. For positive field values, the transferred charge between each adsorbate and  
338 the metal surface decreases, while a negative field value has the opposite effect. By  
339 combining this information with the bond strength of the MSR intermediates in Fig. 3, we  
340 find that the stronger bond strength of the intermediates correlates well with the amount  
341 of charge transferred between the metal surface and the adsorbates. For example, upon  
342 adsorption of a  $\text{CH}_2\text{O}$  molecule in the presence of an applied field the charge transferred  
343 between Ni surface and  $\text{CH}_2\text{O}$  adsorbate decreases by  $\sim 0.3 e$  as one increases the field  
344 value from  $-1 \text{ V/\AA}$  to  $1 \text{ V/\AA}$ . This mirrors the fact that the adsorption energy of  $\text{CH}_2\text{O}$  is  
345 monotonically weakened as one varies the field strength from  $-1 \text{ V/\AA}$  to  $1 \text{ V/\AA}$ .

346 The adsorption of  $\text{CH}_2\text{OH}$  is an exception, since the adsorption energy of a  
347  $\text{CH}_2\text{OH}$  molecule becomes weaker with a negative field but the amount of charge  
348 transferred increases in such an environment. As shown in Fig. S14, combining the Bader  
349 charge analysis and the differential charge density, it shows that the presence of a  
350 positive electric field polarizes the surface with partially positive charge, which has a  
351 Coulomb attraction with the partial negative charged O atom of the  $\text{CH}_2\text{OH}$  molecule and  
352 further strengthens the adsorption of this molecule. On the other hand, a negative electric  
353 field polarizes the surface with partial negative charge, which has a Coulomb repulsion  
354 with the partial negative charge of the O atom in the  $\text{CH}_2\text{OH}$  molecule and further  
355 weakens the adsorption of this molecule. This corresponds well with our calculations  
356 where the adsorption energy of a  $\text{CH}_2\text{OH}$  molecule over a Ni(111) surface with a  
357 negative field is much weaker than the ones with a positive field based on the Coulomb

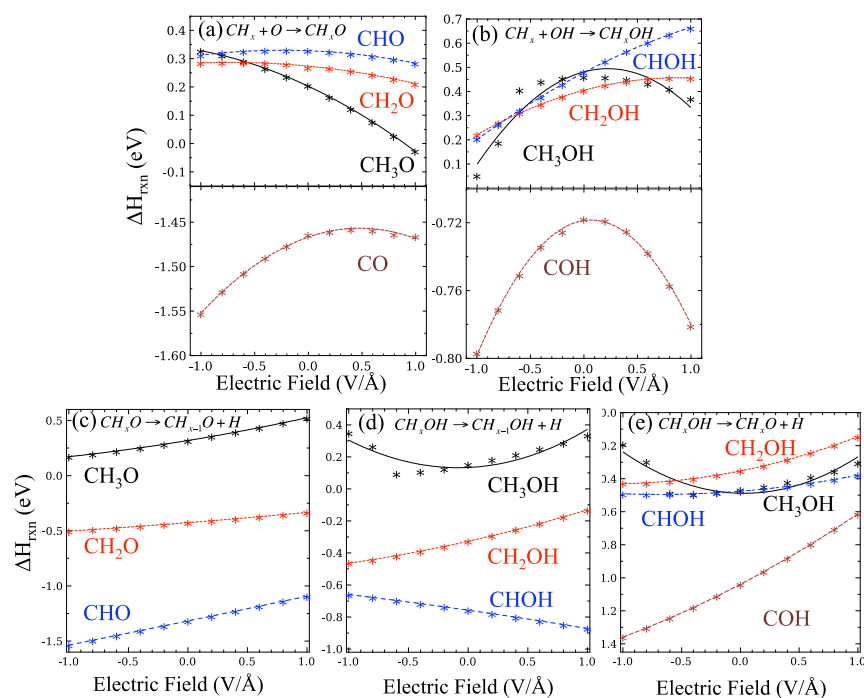
358 forces. In addition, with a positive electric field, two H atoms (bonded to the C atom) are  
359 partially positively charged, which form two internal dipole moments with the bonded C  
360 atom (see Fig. S14). The direction of the dipole moments of the C-H bonds aligns with a  
361 positive electric field, which further stabilizes the system. On the other hand, the  
362 direction of the dipole moments of the C-H bonds is not aligned with the negative electric  
363 field. As such, a negative electric field leads the majority of the transferred charges to be  
364 from the metal slab to two H atoms (bonded to the C atoms). Consequently, there is no  
365 internal dipole moment between the C and H atoms. This leads to a weaker adsorption of  
366 the molecule as compared to when a positive field is present even though the total  
367 amount of transferred charges (0.34 e) with a negative field is more than that in the  
368 presence of a positive electric field (0.13 e).

369 Overall, an electric field notably affects the adsorption of the MSR-involved  
370 species on a Ni(111) surface and consequently changes the underlying energy landscape  
371 involved in the such a reaction. The field effects can be rationalized through an analysis  
372 of the effective dipole moments, the electronic geometries, the DOS, and differential  
373 charge densities of the adsorbed species. Their transferred charges are quantified with a  
374 Bader charge analysis between the adsorbate and metal surface. This further enhances our  
375 understanding of the underlying interactions between the MSR-involved species and a Ni  
376 catalyst surface in the presence of an electric field.

### 377 3.3. MSR reaction energies in the presence of the electric fields

378 The reaction energy ( $\Delta H_{\text{rxn}}$ ) is a key element needed to determine the underlying  
379 reaction pathway. From Section 3.1 and 3.2, it is clear that the presence of a field  
380 significantly changes the electronic interactions between the intermediates and the metal

381 surface. Here, we examine how an electric field influences the reaction energies of each  
 382 possible elementary reaction that could be involved in the underlying MSR operation (Fig.  
 383 5). Co-adsorption occurs for either the initial state (IS), in the case of synthetic  
 384 elementary reaction steps; or the final state (FS), in the case of dissociative elementary  
 385 reaction steps. Such information can also help estimate the field-dependent activation  
 386 energy of each elementary reaction and determine the most favorable pathway in the  
 387 presence of an electric field if one constructs a Brønsted-Evans-Polanyi (BEP) relation  
 388 [57-60] in which the activation energy is linearly correlated with  $\Delta H_{\text{rxn}}$  [61, 62]. Details  
 389 with respect to the most favorable co-adsorption configurations of the FS and IS for each  
 390 possible elementary reaction in the absence of an electric field are shown in Fig. S9 and  
 391 their corresponding reaction energies with no fields (calculated by Eq. (6)) are  
 392 summarized in Table S4.



393

394 **Fig. 5.** The field-dependent reaction energy trendlines of different elementary reactions proposed  
 395 in Fig. 1 in the presence of different electric fields on a Ni(111) surface. The dots represent their

396 adsorption energies under a particular electric field strength ranging from  $-1 \text{ V/\AA}$  to  $1 \text{ V/\AA}$  at an  
397 interval of  $0.2 \text{ V/\AA}$ .

### 398 3.3.1. Dehydrogenation of $\text{CH}_x$ and $\text{H}_x\text{O}$ species with different electric fields

399 As Fig. 1 shows, the MSR reaction starts with the dehydrogenation of the  $\text{CH}_4$   
400 and the  $\text{H}_2\text{O}$  reactants. From Section 3.1, we know that  $\text{CH}_4$  is very weakly adsorbed on  
401 the surface, and it prefers to dissociate to form  $\text{CH}_3$  with H. The reaction energy for  
402  $\text{CH}_4 \rightarrow \text{CH}_3 + \text{H}$  is nearly energy neutral. As we vary the field value from  $-1 \text{ V/\AA}$  to  $1$   
403  $\text{V/\AA}$ , the reaction energy decreases from  $0.24 \text{ eV}$  to  $-0.03 \text{ eV}$ . This has an opposite field  
404 effect as compared to the dehydrogenation reaction energies of the other  $\text{CH}_x$  groups  
405 ( $x=1\sim 3$ ). Similarly, the changes of the dipole moments (Table 2) associated with the  
406 dehydrogenation of the  $\text{CH}_x$  ( $x=1\sim 3$ ) species are of opposite sign to those involved for  
407 the dehydrogenation of  $\text{CH}_4$ . From our previous work [29], we know that a positive  
408 electric field doesn't largely alter the dehydrogenation of the  $\text{CH}_3$  and the  $\text{CH}_2$  species,  
409 but that it does alter the  $\text{CH} \rightarrow \text{C} + \text{H}$  reaction by raising its reaction barrier, which  
410 suppresses pure carbon formation. Early investigations [31] also showed that a negative  
411 electric field can accelerate the dehydrogenation of  $\text{H}_2\text{O}$  to form surface OH and O  
412 species, while a positive electric field can hinder its dehydrogenation. This fundamental  
413 information can guide us toward the design of a new electrocatalytic MSR operation to  
414 prevent coking and enhance the efficient utilization of steam: it is better to perform water  
415 dehydrogenation in the presence of a negative electric field in one step, and methane  
416 dissociation in the presence of a positive electric field as the other step. In this way,  
417 sufficient surface OH and O species can be produced, which can oxidize the  $\text{CH}_x$  ( $x=1\sim 3$ )  
418 groups to form  $\text{CH}_x\text{OH}$  and  $\text{CH}_x\text{O}$  species and further prevent coking.

### 419 3.3.2. Electric field effects on the formation of $\text{CH}_x\text{O}$ and $\text{CH}_x\text{OH}$ species.

420  $\text{CH}_x$  ( $x = 0\sim 3$ ) segments can get oxidized with OH and O, which can then form  $\text{CH}_x\text{O}$   
421 and  $\text{CH}_x\text{OH}$  species on Ni(111). Except for the formation of CO and COH, the formation  
422 energies of other  $\text{CH}_x\text{O}$  ( $\sim 0.3$  eV) and  $\text{CH}_x\text{OH}$  ( $\sim 0.42$  eV) species are all endothermic.  
423 Additionally, the formation energies of CHO and CHOH are much smaller than those  
424 involved in the dissociation of a CH molecule. As a result, an CH intermediate seems to  
425 prefer to be oxidized by surface OH or O species rather than dissociating to a pure C  
426 atom. The formation of COH and CO from pure C atoms on a Ni(111) surface are both  
427 exothermic, which suggests that even though pure carbon atoms may form on Ni(111),  
428 sufficient surface O or OH segments can prevent the formation of coke as well.

429 After one applies an electric field to the most favorable co-adsorption  
430 configurations involving the  $\text{CH}_x$  and the O species to the corresponding  
431  $\text{CH}_x + \text{O} \rightarrow \text{CH}_x\text{O}$  reactions, we find that the reaction involving the formation of  $\text{CH}_3\text{O}$   
432 has the most significant field effect (Fig. 5(a)). This can also be checked in Table 2,  
433 wherein the formation of  $\text{CH}_3\text{O}$  has the largest effective dipole moment with a value of  
434  $0.19$  eV $\cdot\text{\AA}/\text{V}$ . In the presence of a field of  $1$  V/ $\text{\AA}$ , the  $\text{CH}_3 + \text{O} \rightarrow \text{CH}_3\text{O}$  reaction is  
435 nearly energy neutral, while the reaction energy monotonically increases by  $\sim 0.4$  eV as  
436 we decrease the electric field values from  $1$  V/ $\text{\AA}$  to  $-1$  V/ $\text{\AA}$ . For the hydroxyl group  
437 oxidation of  $\text{CH}_x$  reactions, the formation energy of CHOH has the largest field effect.  
438 The reaction energy of the  $\text{CH} + \text{OH} \rightarrow \text{CHOH}$  reaction monotonically increases by  
439  $\sim 0.5$  eV as we increase the electric field strengths from  $-1$  V/ $\text{\AA}$  to  $1$  V/ $\text{\AA}$  (Fig. 5(b)).  
440 Therefore, based on the BEP linearly correlations,  $\text{CH}_x$  species are easier to be oxidized  
441 by a hydroxyl group than that by a surface oxygen species in the presence of a negative

442 electric field, while a positive electric field has an opposite effect. This indicates that with  
443 different electric fields, the overall MSR reaction mechanism can be modified.

### 444 3.3.3. Dehydrogenation of $\text{CH}_x\text{O}$ and $\text{CH}_x\text{OH}$ species in the presence of a field.

445 Fig. 5(c) shows how an electric field has the similar effects on breaking the C-H  
446 bond for all the  $\text{CH}_x\text{O}$  species, in which a negative field drives the  $\Delta H_{\text{rxn}}$  values for its  
447 dehydrogenation to  $\text{CH}_{x-1}\text{O}$  to much smaller values as compared to when a positive  
448 electric field is applied. Comparing the  $\Delta d_{F=0}$  values for the  $\text{CH}_x\text{O}$  dehydrogenation  
449 reactions (Table 2) one can see that the CHO dehydrogenation has the greatest field effect:  
450 its reaction energy increases by  $\sim 0.5$  eV when one increases the field value from  $-1$  V/Å  
451 to  $1$  V/Å. Interestingly, since the dehydrogenation of the  $\text{CH}_x\text{O}$  species has C-H cleavage,  
452 the field effects on the reaction energies of its dehydrogenation to  $\text{CH}_{x-1}\text{O}$  reactions are  
453 similar to the ones for the methyl dehydrogenation from our previous work [29].

454 Dehydrogenation of  $\text{CH}_x\text{OH}$  can either break the C-H bond (Fig. 5(d)) or break  
455 the O-H bond (Fig. 5(e)). For methanol, the breaking of the C-H bond via the  
456  $\text{CH}_3\text{OH} \rightarrow \text{CH}_3\text{O} + \text{H}$  reaction is endothermic with a  $\Delta H_{\text{rxn}}$  value of  $0.15$  eV. The  
457 reaction energy increases by  $0.24$  eV when one increases the field value from  $-1$  V/Å to  $1$   
458 V/Å. On the other hand, the breaking the O-H bond in a methanol molecule to form a  
459  $\text{CH}_3\text{O}$  is exothermic with a  $\Delta H_{\text{rxn}}$  value of  $-0.47$  eV. The electric field effects on this  
460 reaction are similar to that on the  $\text{CH}_3\text{OH} \rightarrow \text{CH}_2\text{OH} + \text{H}$  reaction. Since the  
461  $\text{CH}_3\text{OH} \rightarrow \text{CH}_3\text{O} + \text{H}$  reaction is exothermic and the  $\text{CH}_3\text{OH} \rightarrow \text{CH}_2\text{OH} + \text{H}$  reaction  
462 is endothermic, we conclude that it is energetically more favorable to break the O-H bond  
463 in a  $\text{CH}_3\text{OH}$  molecule. In particular, a negative electric field of  $-0.6$  V/Å further makes  
464 the O-H bond breaking more exothermic. A similar analysis can be applied for the C-H

465 and O-H bond breaking of CH<sub>2</sub>OH and CHOH. The O-H bond breaking of CH<sub>2</sub>OH is  
466 more energetically favorable than its counterpart C-H bond breaking in the presence of a  
467 field value of -1 V/Å. Moreover, the C-H bond breaking of CHOH is ~0.3 eV more  
468 exothermic and has a larger field influence than the breaking of the O-H bond.  
469 Furthermore, O-H bond breaking of a COH molecule is the most exothermic reaction  
470 among all the dehydrogenation reactions of the CH<sub>x</sub>OH species, with a ΔH<sub>rxn</sub> value of -  
471 1.04 eV. Additionally, the *COH* → *CO* + *H* reaction has the greatest electric field effect  
472 as well, in which the reaction energy of the *COH* → *CO* + *H* reaction monotonically  
473 increases from -1.36 eV to -0.61 eV as we increase a field value from -1 V/Å to 1 V/Å.

474 Overall, for the formation of CH<sub>x</sub>O or CH<sub>x</sub>OH, a positive electric field facilitates  
475 the oxygen oxidation of the CH<sub>x</sub> species, while a negative electric field accelerates the  
476 hydroxyl oxidation of the CH<sub>x</sub> species. We also examined the C-H or O-H bond breaking  
477 of these species and found that these bond breaking reaction energies are much smaller  
478 than their formation energies and also had larger field effects. Except for CHOH, the  
479 dehydrogenation of the other CH<sub>x</sub>O and CH<sub>x</sub>OH species has similar field effects: a  
480 negative electric field lowers the ΔH<sub>rxn</sub> values and a positive field enlarges the ΔH<sub>rxn</sub>  
481 values. Comparing the dehydrogenation reactions of CH<sub>x</sub>O and CH<sub>x</sub>OH, the reactions  
482 having larger field dependences are in following order *COH* → *CO* + *H* >  
483 *CHO* → *CO* + *H* > *CH<sub>3</sub>O* → *CH<sub>2</sub>O* + *H* .

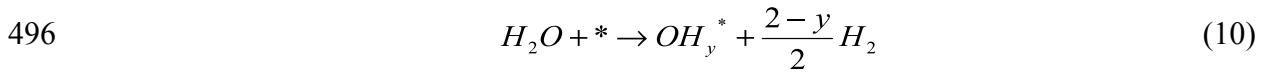
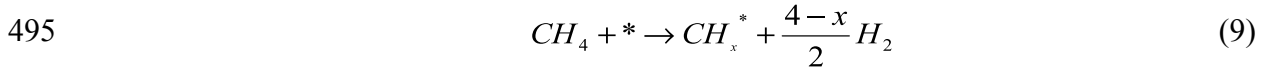
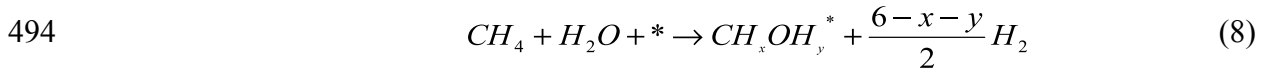
#### 484 3.4. Phase diagram from first principles of MSR intermediates

##### 485 3.4.1. Phase diagram.

486 The change of Gibbs free energy of adsorption (ΔG) as a function of the hydrogen  
487 chemical potential (Δμ<sub>H</sub>) and the electric field strength (*F*) can provide us with a  
488 connection between our DFT calculations and the relative equilibrium stabilities of the

489 possible MSR intermediates under various experimental conditions [63-66]. The  
 490 following paragraph explains how we define  $\Delta G$  based on our first principles calculations.

491 The formation of the  $CH_xOH_y$  ( $y = 0$  or  $1$ ),  $CH_x$  and  $OH_y$  species on Ni(111)  
 492 under MSR conditions is shown in Eq. (8)-(10) and the binding energy ( $E_b^{CH_xOH_y^*}$ ,  $E_b^{CH_x^*}$ ,  
 493  $E_b^{OH_y^*}$ ) is defined in Eq. (11)-(13).



$$497 \quad E_b^{CH_xOH_y^*} = E_{CH_xOH_y^*} + \frac{6-x-y}{2} E_{H_2} - E_* - E_{CH_4} - E_{H_2O} \quad (11)$$

$$498 \quad E_b^{CH_x^*} = E_{CH_x^*} + \frac{4-x}{2} E_{H_2} - E_* - E_{CH_4} \quad (12)$$

$$499 \quad E_b^{OH_y^*} = E_{OH_y^*} + \frac{2-y}{2} E_{H_2} - E_* - E_{H_2O} \quad (13)$$

500 Where  $E_{CH_xOH_y^*}$ ,  $E_{CH_x^*}$ ,  $E_{OH_y^*}$  are the total energies of the isolated intermediates ( $CH_xOH_y$ ,  
 501  $CH_x$ ,  $OH_y$ ) on the top of a Ni(111) surface and ‘\*’ stands for a clean Ni(111) slab, while  
 502  $E_{H_2}$ ,  $E_{CH_4}$ , and  $E_{H_2O}$  represent the gas phase energies of  $H_2$ ,  $CH_4$  and  $H_2O$ , respectively.  
 503  $\Delta G$  is then obtained by Eq. (14)-(16) [64, 66].

$$504 \quad \Delta G = E_b^{CH_xOH_y^*} + (6-x-y)\Delta\mu_H - \Delta\mu_{CH_4} - \Delta\mu_{H_2O} \quad (14)$$

$$505 \quad \Delta G = E_b^{CH_x^*} + (4-x)\Delta\mu_H - \Delta\mu_{CH_4} \quad (15)$$

$$506 \quad \Delta G = E_b^{OH_y^*} + (2-y)\Delta\mu_H - \Delta\mu_{H_2O} \quad (16)$$



507 Where  $\Delta\mu_H$  is defined as  $\Delta\mu_H = \mu_H - \frac{1}{2}E_{(H_2)}$  since we take  $H_2$  as the hydrogen reference.

508 Similarly, we can also get  $\Delta\mu_{CH_4}$  and  $\Delta\mu_{H_2O}$ . At 0 K and standard pressure conditions, we

509 define  $\mu_H(0K, p_0^{H_2}) = \frac{1}{2}E_{(H_2)} \equiv 0$ .

510 From above paragraphs, we have completely described how we obtain  $\Delta G$  from  
511 our DFT calculations as a function of  $\Delta\mu_H$ . The next step is to relate the  $\Delta\mu_H$  to our  
512 realistic temperature and hydrogen partial pressure. Via the formula for a pure ideal gas  
513 (i.e.  $H_2$ ) (Eq. (17)), we can include the effect of pressure and temperature on  $\Delta\mu_H$ . Here  
514 we assume that  $2H \rightarrow H_2$  is at equilibrium.

$$515 \quad \Delta\mu_H(T, p^{H_2}) = \Delta\mu_H(T, p_0^{H_2}) + \frac{1}{2}k_B T \ln \frac{p}{p_0} \quad (17)$$

516 Where  $p^{H_2}$  and  $p_0^{H_2}$  represent the practical partial pressure and standard partial pressure  
517 of  $H_2$ , and  $k_B$  is the Boltzmann's constant. This equation provides us with a description of  
518 how the hydrogen chemical potential is altered by the pressure at a certain temperature.

519 Additionally, we also have to figure out how to obtain the value of  $\Delta\mu_H(T, p_0^{H_2})$ . With

520 respect to  $\mu_H(0K, p_0^{H_2})$ ,  $\mu_H(T, p_0^{H_2})$  is given in Eq. (18). The values of enthalpy H and

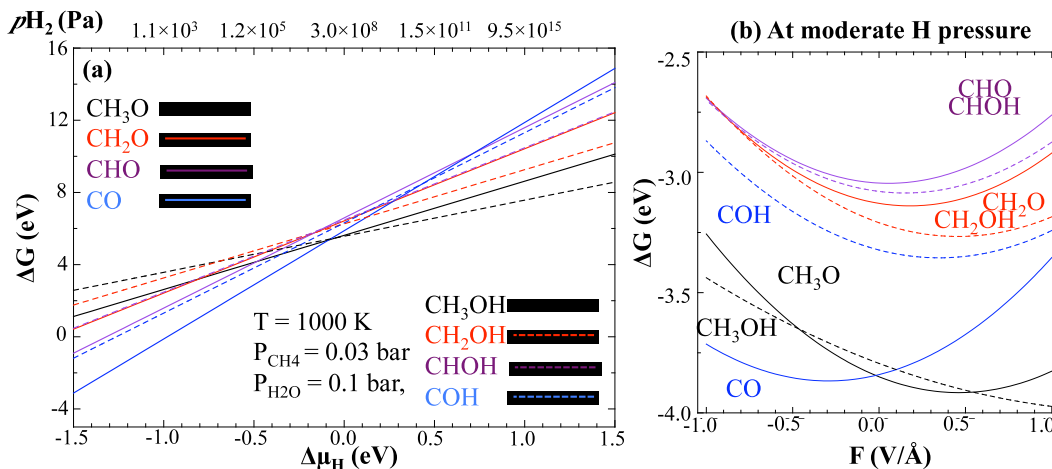
521 entropy S at a certain temperature and standard pressure can be found in Thermodynamic

522 Tables [67]. Since  $\mu_H(0K, p_0^{H_2}) = \frac{1}{2}E_{(H_2)} \equiv 0$ , we can get  $\Delta\mu_H(T, p_0^{H_2})$ . Similar to

523  $\Delta\mu_H(T, p_0^{H_2})$ , we can calculate the values of  $\Delta\mu_{CH_4}(T, p)$  and  $\Delta\mu_{H_2O}(T, p)$  as well.

$$524 \quad \mu_H(T, p_0^{H_2}) = \frac{1}{2}[H(T, p_0^{H_2}) - H(0K, p_0^{H_2})] - \frac{1}{2}T[S(T, p_0^{H_2}) - S(0K, p_0^{H_2})] \quad (18)$$

525 Fig. 6(a) shows that in the absence of the electric fields,  $\Delta G$  for  $\text{CH}_x\text{OH}$  and  
 526  $\text{CH}_x\text{O}$  at 1000 K as a function of hydrogen chemical potential. In order to prevent coking,  
 527 experimenters keep the partial pressure ratio of  $\text{H}_2\text{O}/\text{CH}_4$  to  $\sim 3$  [68]. A lower value of  $\Delta G$   
 528 indicates that the conformation is more stable on the Ni(111) surface. When the field is  
 529 absent, the more hydrogenated species ( $\text{CH}_x\text{OH}$ ) are stabilized as hydrogen pressure is  
 530 increased. When the hydrogen partial pressure is low, CO, CHO and COH are the most  
 531 stable species on Ni(111). For high hydrogen partial pressure values,  $\text{CH}_3\text{OH}$  and  $\text{CH}_3\text{O}$   
 532 are more likely to stay on the surface. But under such high temperature conditions, it  
 533 would be hard to obtain methanol as a product from the reactor since after its desorption,  
 534 gas phase methanol decomposes easily into carbons and hydrogen gas [69]. It is also  
 535 worth mentioning that even if we change the partial pressures or the  $\text{H}_2\text{O}/\text{CH}_4$  ratio, the  
 536 relative stabilities of the MSR-involved species won't change at given temperature.



537

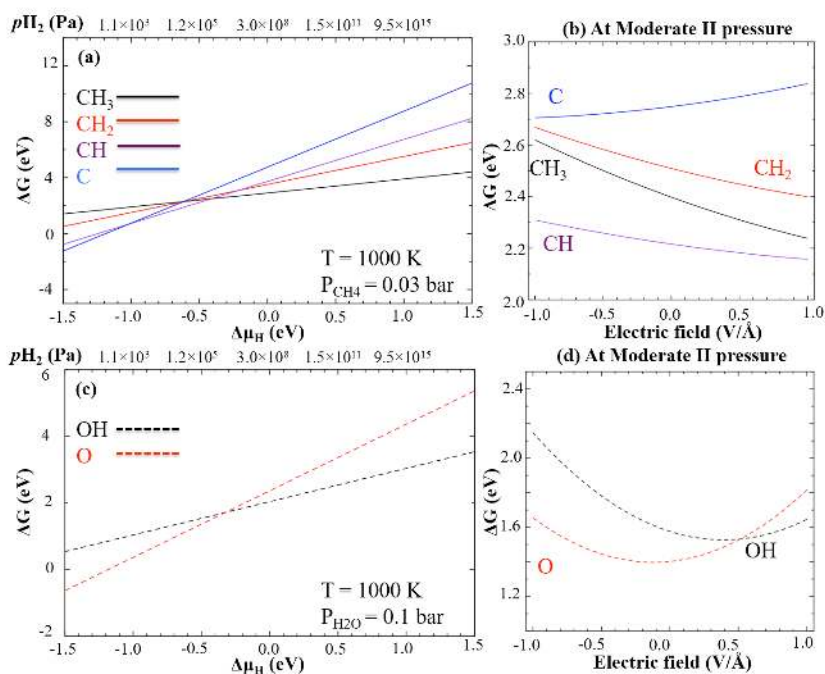
538 **Fig. 6.** Phase diagram from first principles representing the relative equilibrium stabilities of the  
 539  $\text{CH}_x\text{O}$  and  $\text{CH}_x\text{OH}$  species as a function of the hydrogen chemical potential and an electric field.  
 540 Part (a) presents the value of  $\Delta G$  as a function of hydrogen partial pressure with no fields. Part (b)  
 541 shows that the Gibbs free energy of adsorption  $\Delta G$  as a function of an electric field of  $-1 \text{ V/\AA}$  to 1

542  $\text{V}/\text{\AA}$  at hydrogen partial pressures of  $\sim 10^6$  Pa. It is also worthy to mention that all the  
543 intermediates we identified here are at a low coverage of  $1/9$  ML.

544 Fig. 7(a) and (c) separately present the relative equilibrium stabilities of  $\text{CH}_x$  and  
545  $\text{OH}_y$  intermediates as the function of the hydrogen partial pressure with no electric fields.  
546 The results clearly show that at low partial pressures of hydrogen, we can obtain surface  
547 C atoms and CH molecules from the dissociation of pure methane, while a  $\text{CH}_3$  molecule  
548 is more likely to occur on the surface as we increase the partial pressure of hydrogen  
549 above  $5 \times 10^6$  Pa. For the dissociation of water, surface oxygen species are stable for low  
550 partial hydrogen pressure values, while hydroxyl species are more stable at high  
551 hydrogen partial pressures. By combining this information with the stability of  $\text{CH}_x\text{OH}_y$   
552 species, we can conclude that at low partial pressures of hydrogen, we can obtain surface  
553 CO, CHO, COH, C, CH and O since they are stable under such applied conditions.  
554 Furthermore, under such conditions, a CO product can be formed from the surface  
555 oxygen oxidation of either an adsorbed C or a surface CH group. On the other hand,  
556 when the hydrogen partial pressure is higher than  $5 \times 10^6$  Pa, the most stable species on the  
557 surface change to  $\text{CH}_3\text{OH}$ ,  $\text{CH}_3\text{O}$ ,  $\text{CH}_3$ , and OH. This suggests that under high hydrogen  
558 partial pressure conditions, the surface methanol species can be obtained from the  
559 oxidation of  $\text{CH}_3$  with adsorbed hydroxyl groups.

560 For different hydrogen chemical potential values, an electric field will play  
561 different roles in the relative equilibrium stability of MSR-involved intermediates. When  
562 the hydrogen chemical potential value is low, a CO molecule on Ni(111) has the lowest  
563 value of  $\Delta G$ . At these conditions, COH and CHO intermediates are also very stable on  
564 the surface as compared to the stabilities of other  $\text{CH}_x\text{O}$  and  $\text{CH}_x\text{OH}$  molecules.  
565 Moreover, due to the large differences of the  $\Delta G$  values for each intermediate value of

566  $\Delta\mu_{\text{H}}$ , the electric field effects are not large enough to alter the order of stability for these  
 567 intermediates. Similarly, in the absence of field,  $\text{CH}_3\text{OH}$  and  $\text{CH}_3\text{O}$  are more likely to be  
 568 observed on Ni(111) when the hydrogen partial pressure is high. An electric field on the  
 569 order of  $-1.0 \text{ V/\AA}$  to  $1.0 \text{ V/\AA}$  also doesn't significantly affect the stability order for  $\text{CH}_x\text{O}$   
 570 and  $\text{CH}_x\text{OH}$  under these conditions. Similarly, when the hydrogen chemical potential  
 571 value is very low or very high, an electric field didn't alter the stability orders of  $\text{CH}_x$  and  
 572  $\text{OH}_y$  species as well.

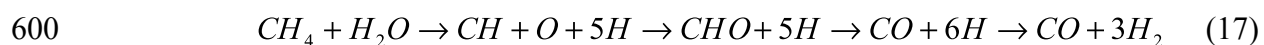


573  
 574 **Fig. 7.** The relative equilibrium stabilities of the  $\text{CH}_x$  and  $\text{OH}_x$  species as a function of the  
 575 hydrogen chemical potential and an electric field. Part (a) presents the value of  $\Delta G$  as a function  
 576 of hydrogen partial pressure in the absence of a field. Part (b) shows  $\Delta G$ , the Gibbs free energy of  
 577 adsorption, as a function of an electric field of  $-1 \text{ V/\AA}$  to  $1 \text{ V/\AA}$  at the same moderate hydrogen  
 578 partial pressures ( $\sim 10^6 \text{ Pa}$ ) that we presented in Fig.7. It is also worthy to mention that all the  
 579 intermediates we identified here are at a low coverage of  $1/9 \text{ ML}$ .

580 On the other hand, at moderate hydrogen partial pressure values of  $\sim 10^6$  Pa (Fig.  
581 6(b), Fig. 7(b) and (d)), the presence of a simulated field can modify the relative stability  
582 of the adsorbates: (i) For  $\text{CH}_x\text{OH}_y$  species, at negative field values CO is the most  
583 favorable species on Ni(111), while methanol becomes much more stable over the  
584 surface as we increase the field value from negative to positive values; (ii) For the  $\text{CH}_x$   
585 species, CH is the most stable species over a Ni surface, while  $\text{CH}_3$  is the second stable  
586 species and becomes much more stable as we apply a large positive electric field; (iii) For  
587 the  $\text{OH}_y$  species at a high positive electric field value at moderate hydrogen partial  
588 pressures, we can get hydroxyl groups on the Ni surface. As a result, the presence of a  
589 high positive electric field can aid in the formation of methanol on Ni(111) via the  
590 reaction of  $\text{CH}_3$  species with hydroxyl groups under certain conditions.

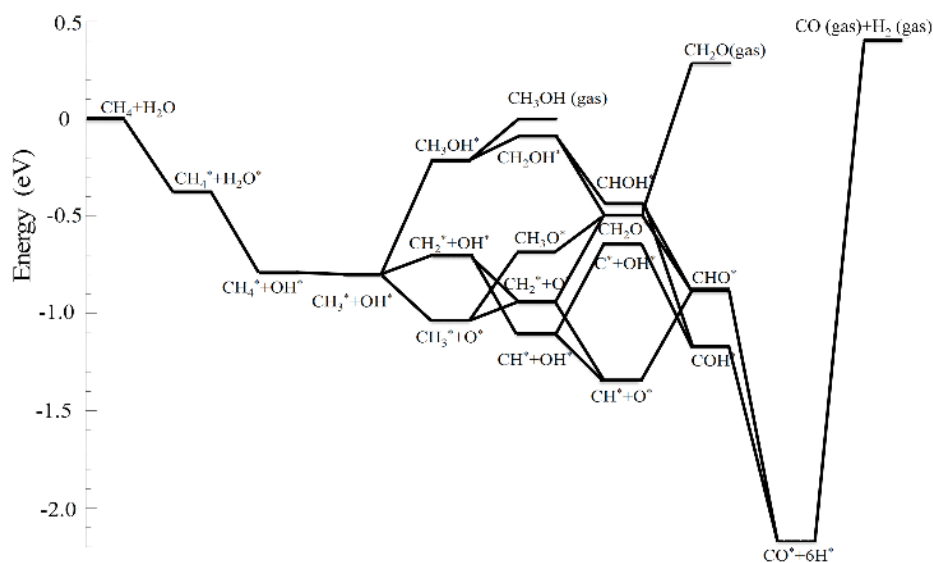
#### 591 3.4.2. Combining phase diagram with thermodynamic scheme.

592 By combining our phase diagram (Fig. 6 and Fig. 7) and thermodynamic scheme  
593 (Fig. 8 and Fig. 9), we can better understand the underlying processes occurring during  
594 the MSR reaction. From section 3.4.1, we know that CO has the lowest  $\Delta G$  at low  
595 hydrogen chemical potential values in the absence of a field. The CO products can be  
596 obtained from the surface oxygen oxidation of either an adsorbed C or a surface CH  
597 group, since these species are thermodynamically stable on a Ni(111) surface under such  
598 conditions. Based on Fig. 8, the lowest energy pathway is shown in Eq. (17), which also  
599 includes CH, O, and CHO intermediates.



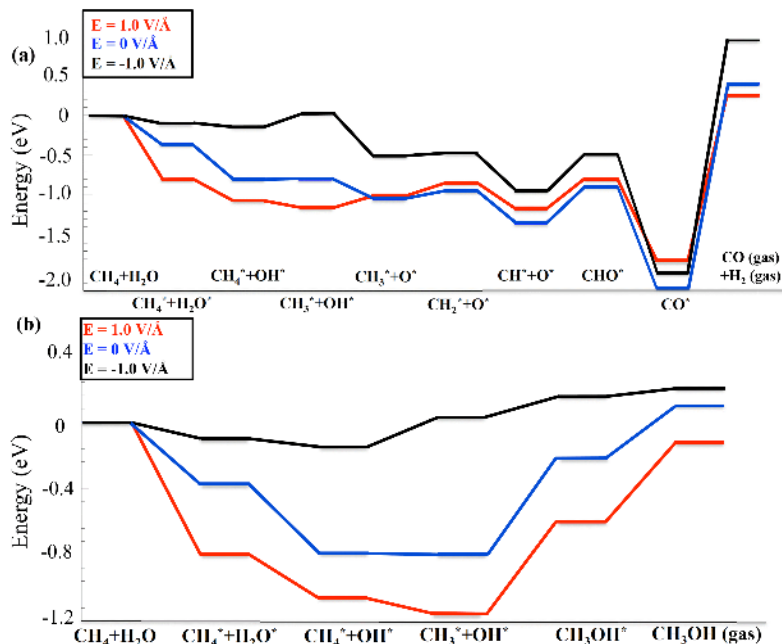
601 We remark that the overall energy profile plotted in Fig. 8 and Fig. 9 for the MSR  
602 reaction are from DFT calculations at 0 K. However, after accounting the entropy effects  
603 (using an MSR operating temperature of 1073 K), the Gibbs free energy changes ( $\Delta G$ ) of

604 a CO molecule from the Ni(111) surface to a gas phase CO molecule in the presence of a  
 605 positive field, in the absence of a field and in the presence of a negative field are only -  
 606 0.35 eV, -0.12 eV and 0.02 eV. We remark that the exothermic values are due to high  
 607 temperatures involved since at room temperature these values would be 1.14 eV, 1.37 eV  
 608 and 1.56 eV, respectively. Consequently, the overall MSR reaction energy profile,  
 609 involving the production of CO and H<sub>2</sub> in the gas phase, reduces from ~3 eV (at 0 K) to  
 610 ~2 eV (at 1073 K). On the other hand, for the surface reactions, such as  
 611  $CH_x^* \rightarrow CH_{x-1}^* + H^*$ ,  $CH_x^* + O^* \rightarrow CH_xO^*$ , the entropy effects on the reaction energies  
 612 at 1073 K are all less than 0.2 eV as compared to the ones at 0 K, which are significantly  
 613 smaller than the phase change steps (i.e. the CO desorption) and will not largely influence  
 614 the overall energy profiles. More details related to the changed Gibbs free energy  
 615 calculations are given in Section 5 in the ESI.



616  
 617 **Fig. 8.** Thermodynamic scheme of all possible mechanisms (see Fig. 1) in MSR reaction over a  
 618 Ni(111) catalysts in the absence of a field. Here we use ‘\*’ to denote when the species are  
 619 adsorbed on a Ni(111) surface.

620 Fig. 9(a) shows the simulated field effects on this lowest energy pathway. A  
621 positive field significantly strengthens the adsorption of reactants, decreases the  
622 desorption energy of the CO and H<sub>2</sub> products, and lowers the overall energy profile.  
623 Therefore, we conclude that a positive electric field improves the MSR processes. On the  
624 other hand, at moderate hydrogen partial pressure values ( $\sim 10^6$  Pa) at field values ranging  
625 from 0.0 V/Å to 0.5 V/Å, we can obtain the surface CH<sub>3</sub>O intermediate. Among the  
626 reaction mechanisms that involve the CH<sub>3</sub>O intermediates, only the  $CH_4 \rightarrow CH_3 + H$   
627 and the  $CH_3 + O \rightarrow CH_3O$  reactions are endothermic. A positive electric field also  
628 further decreases the reaction energies of these two reactions and causes these two  
629 reactions to become slightly exothermic. Thus, from the perspective of only the reaction  
630 energy, the CH<sub>3</sub>O-involved reaction mechanisms are likely to occur in the presence of a  
631 positive field ranging from 0.0 V/Å to 0.5 V/Å and at moderate hydrogen partial pressure  
632 values. Additionally, after increasing the field from 0.5 V/Å to 1 V/Å, we can obtain  
633 methanol on Ni(111). From Fig. 9(b), it is also clearly shown that the presence of a  
634 positive field can lower the overall energy profile of forming methanol. This information  
635 can help us select a reduced number of elementary reactions from such a potentially  
636 complex overall MSR reaction mechanism when calculating reaction energy barriers, as  
637 shown in Fig. 1.



638

639 **Fig. 9.** The lowest energy pathway in the presence and absence of an electric field (a) and the  
 640 reaction pathway for forming methanol via hydroxyl oxidation of CH<sub>3</sub> species (b).

## 641 6. Conclusion

642 We thoroughly investigated the electric field on the adsorption the MSR-involved  
 643 species as well as its influence on the reaction energies of all possible MSR elementary  
 644 reactions. In our adsorption study in the presence of a simulated field we found that the  
 645 effect of an electric field on MSR-involved chemisorbed species are similar. Such a  
 646 conclusion was obtained through our projected density of states, differential charge  
 647 density and Bader charge analysis. The field-dependent adsorption strength of MSR  
 648 intermediates based on the effective dipole moment analysis was found to be as follows:  
 649  $CH_xO > CH_xOH > H_xO > CH_x$ . On the other hand, the formation of CH<sub>x</sub>O and CH<sub>x</sub>OH  
 650 was found to be more rates dominating than their corresponding dehydrogenation  
 651 reactions. With a positive field, surface O atom oxidation of CH<sub>x</sub> species is more likely to



652 occur, while with a negative field, surface hydroxyl group oxidation of  $\text{CH}_x$  is more  
653 likely to occur.

654         The phase diagram that was constructed from first principles provides the relative  
655 equilibrium stabilities of the possible MSR intermediates as a function of both the  
656 hydrogen partial pressure and a tunable electric field strength under realistic experimental  
657 conditions. This provides us the most likely occurring MSR mechanisms at moderate  
658 hydrogen partial pressures, where CO can be obtained with a negative field, while the  
659  $\text{CH}_3\text{OH}$  can be found over the surface for positive field values. For the most favorable  
660 reaction mechanisms with different hydrogen pressures, the overall energy profiles are  
661 further lowered in the presence of a positive electric field. In summary, our  
662 computational results enhance our understanding of the catalytic MSR reaction  
663 mechanisms in the presence of tunable electric fields. The information provided here also  
664 points us toward the selection of the elementary reactions for further kinetic studies of the  
665 methane steam reforming reaction mechanism. By combining this study with our previous  
666 work, we conclude that a positive electric field can significantly reduce the formation of  
667 coke, lower the lowest energy path, stabilize the adsorption of reactants, and assist the  
668 desorption of products on a Ni catalyst. For the future work, it is necessary to establish a  
669 microkinetic model for such a catalytic MSR reaction with tunable electric fields in order  
670 to capture the electric field effects for the conversion of methane during the MSR process,  
671 the temperature requirements of the said reaction, the coke formation and the  
672 identification of intermediates as the function of time. By the end, the established  
673 microkinetic model will provide a better guidance of designing a new Ni-based

674 electrocatalytic methane steam reforming process with lower operating temperatures and  
675 higher coke resistance.

## 676 **7. Acknowledgments**

677         We gratefully acknowledge our support by institutional funds provided to JSM  
678 from the Voiland School of Chemical Engineering and Bioengineering. We also thanks to  
679 USDA/NIFA that partial work was under support through the Hatch Project #WNP00807  
680 titled: “Fundamental and Applied Chemical and Biological Catalysts to Minimize  
681 Climate Change, Create a Sustainable Energy Future, and Provide a Safer Food Supply”.  
682 Our thanks also go to the donors of The American Chemical Society Petroleum Research  
683 Fund for partial support. Furthermore, parts of our computational resources were  
684 provided by the Center for Nanoscale Materials at Argonne National Laboratory. Use of  
685 the Center for Nanoscale Materials was supported by the U.S. Department of Energy,  
686 Office of Science, Office of Basic Energy Sciences. We also acknowledge Mr. Gregory  
687 B. Collinge for his helpful comments.

- 689 [1] A.B. Stambouli, E. Traversa, *Renewable Sustainable Energy Rev.*, 6 (2002) 433-455.  
690 [2] J. Sun, X.-P. Qiu, F. Wu, W.-T. Zhu, *Int. J. Hydrogen Energy*, 30 (2005) 437-445.  
691 [3] M.L. Andrade, L. Almeida, M. do Carmo Rangel, F. Pompeo, N. Nichio, *Chem. Eng.*  
692 *Technol.*, 37 (2014) 343-348.  
693 [4] B.V. Merinov, J.E. Mueller, A.C.T. van Duin, Q. An, W.A. Goddard, *J. Phys. Chem. Lett.*, 5  
694 (2014) 4039-4043.  
695 [5] D. Mogensen, J.D. Grunwaldt, P.V. Hendriksen, K. Dam-Johansen, J.U. Nielsen, *J. Power*  
696 *Sources*, 196 (2011) 25-38.  
697 [6] M. Andersson, H. Paradis, J. Yuan, B. Sundén, *Int. J. Energy Res.*, 35 (2011) 1340-1350.  
698 [7] D. Pakhare, J. Spivey, *Chem. Soc. Rev.*, 43 (2014) 7813-7837.  
699 [8] S.D. Angeli, G. Monteleone, A. Giaconia, A.A. Lemonidou, *Int. J. Hydrogen Energy* 39  
700 (2014) 1979-1997.  
701 [9] K. Supat, S. Chavadej, L.L. Lobban, R.G. Mallinson, *Ind. Eng. Chem. Res.*, 42 (2003) 1654-  
702 1661.  
703 [10] J. Sehested, J.A.P. Gelten, I.N. Remediakis, H. Bengaard, J.K. Nørskov, *J. Catal.*, 223 (2004)  
704 432-443.  
705 [11] J. Sehested, *Catal. Today*, 111 (2006) 103-110.  
706 [12] K. Ahmed, K. Foger, *Catal. Today*, 63 (2000) 479-487.  
707 [13] J. Liu, B.D. Madsen, Z. Ji, S.A. Barnett, *Electrochem. Solid-State Lett.*, 5 (2002) A122-  
708 A124.  
709 [14] M.N. Barroso, A.E. Galetti, M.C. Abello, *Appl. Catal., A*, 394 (2011) 124-131.  
710 [15] S. Adhikari, S. Fernando, S.R. Gwaltney, S.D. Filip To, R. Mark Bricka, P.H. Steele, A.  
711 Haryanto, *Int. J. Hydrogen Energy*, 32 (2007) 2875-2880.  
712 [16] A.M. Gadalla, B. Bower, *Chem. Eng. Sci.*, 43 (1988) 3049-3062.  
713 [17] S. Adhikari, S. Fernando, A. Haryanto, *Energy Fuels*, 21 (2007) 2306-2310.  
714 [18] K. Hou, R. Hughes, *Chemical Engineering Journal*, 82 (2001) 311-328.  
715 [19] J. Comas, F. Mariño, M. Laborde, N. Amadeo, *Chem. Eng. J.*, 98 (2004) 61-68.  
716 [20] G. Jones, J.G. Jakobsen, S.S. Shim, J. Kleis, M.P. Andersson, J. Rossmeisl, F. Abild-  
717 Pedersen, T. Bligaard, S. Helveg, B. Hinnemann, J.R. Rostrup-Nielsen, I. Chorkendorff, J.  
718 Sehested, J.K. Nørskov, *J. Catal.*, 259 (2008) 147-160.  
719 [21] H.S. Bengaard, J.K. Nørskov, J. Sehested, B.S. Clausen, L.P. Nielsen, A.M. Molenbroek,  
720 J.R. Rostrup-Nielsen, *J. Catal.*, 209 (2002) 365-384.  
721 [22] R.C. Weast, *CRC Handbook of Chemistry and Physics*, CRC Press, Boca Raton, FL, 1983.  
722 [23] D.W. Blaylock, T. Ogura, W.H. Green, G.J.O. Beran, *J. Phys. Chem. C*, 113 (2009) 4898-  
723 4908.  
724 [24] J.R. Rostrup-Nielsen, *Phys. Chem. Chem. Phys.*, 3 (2001) 283-288.  
725 [25] S.-G. Wang, X.-Y. Liao, J. Hu, D.-B. Cao, Y.-W. Li, J. Wang, H. Jiao, *Surf. Sci.*, 601 (2007)  
726 1271-1284.  
727 [26] C.F. Gorin, E.S. Beh, M.W. Kanan, *J. Am. Chem. Soc.*, 134 (2012) 186-189.  
728 [27] Y. Sekine, M. Haraguchi, M. Tomioka, M. Matsukata, E. Kikuchi, *J. Phys. Chem. A*, 114  
729 (2009) 3824-3833.  
730 [28] Y. Sekine, M. Haraguchi, M. Matsukata, E. Kikuchi, *Catal. Today*, 171 (2011) 116-125.  
731 [29] F. Che, R. Zhang, A.J. Hensley, S. Ha, J.-S. McEwen, *Phys. Chem. Chem. Phys.*, 16 (2014)  
732 2399-2410.  
733 [30] F. Che, A.J. Hensley, S. Ha, J.-S. McEwen, *Catal. Sci. Technol.*, 4 (2014) 4020-4035.  
734 [31] F. Che, J.T. Gray, S. Ha, J.-S. McEwen, *J. Catal.*, 332 (2015) 187-200.  
735 [32] J. Neugebauer, M. Scheffler, *Phys. Rev. B*, 46 (1992) 16067-16080.  
736 [33] J.-S. Filhol, M. Neurock, *Angew. Chem. Int. Ed.*, 45 (2006) 402-406.  
737 [34] C.D. Taylor, S.A. Wasileski, J.-S. Filhol, M. Neurock, *Phys. Rev. B*, 73 (2006) 165402.

738 [35] H.J. Kreuzer, R.L.C. Wang, *Philos. Mag. B*, 69 (1994) 945-955.  
739 [36] G. Pacchioni, J.R. Lomas, F. Illas, *J. Mol. Catal. A: Chem.*, 119 (1997) 263-273.  
740 [37] E.M. Stuve, *Chem. Phys. Lett.*, 519-520 (2012) 1-17.  
741 [38] K.-Y. Yeh, M.J. Janik, CHAPTER 3 Density Functional Theory Methods for  
742 Electrocatalysis, *Computational Catalysis*, The Royal Society of Chemistry 2014, pp. 116-156.  
743 [39] K.-Y. Yeh, S.A. Wasileski, M.J. Janik, *Phys. Chem. Chem. Phys.*, 11 (2009) 10108-10117.  
744 [40] A.E. Bolzán, A.C. Chialvo, A.J. Arvia, *J. Electroanal. Chem. Interfacial Electrochem.*, 179  
745 (1984) 71-82.  
746 [41] K. Walter, O.V. Buyevskaya, D. Wolf, M. Baerns, *Catal. Lett.*, 29 (1994) 261-270.  
747 [42] D. Qin, J. Lapszewicz, X. Jiang, *J. Catal.*, 159 (1996) 140-149.  
748 [43] E. Shustorovich, *The Bond-Order Conservation Approach to Chemisorption and*  
749 *Heterogeneous Catalysis: Applications and Implications*, in: H.P. D.D. Eley, B.W. Paul (Eds.)  
750 *Advances in Catalysis*, Academic Press 1990, pp. 101-163.  
751 [44] J. Wellendorff, T.L. Silbaugh, D. Garcia-Pintos, J.K. Nørskov, T. Bligaard, F. Studt, C.T.  
752 Campbell, *Surf. Sci.*, 640 (2015) 36-44.  
753 [45] J. White, D. Bird, *Phys. Rev. B*, 50 (1994) 4954-4957.  
754 [46] J.P. Perdew, K. Burke, M. Ernzerhof, *Phys. Rev. Lett.*, 77 (1996) 3865-3869.  
755 [47] J.P. Perdew, Y. Wang, *Phys. Rev. B*, 45 (1992) 13244-13249.  
756 [48] M.C. Payne, T.A. Arias, J.D. Joannopoulos, *Rev. Mod. Phys.*, 64 (1992) 1045-1097.  
757 [49] P.J. Feibelman, *Phys. Rev. B*, 64 (2001) 125403.  
758 [50] S. Grundner, M.A.C. Markovits, G. Li, M. Tromp, E.A. Pidko, E.J.M. Hensen, A. Jentys, M.  
759 Sanchez-Sanchez, J.A. Lercher, *Nat. Commun.*, 6 (2015).  
760 [51] E. Masumian, S.M. Hashemianzadeh, A. Nowroozi, *Phys. Lett. A*, 378 (2014) 2549-2552.  
761 [52] J.S. McEwen, P. Gaspard, T. Visart de Bocarmé, N. Kruse, *J. Phys. Chem. C*, 113 (2009)  
762 17045-17058.  
763 [53] J.S. Filhol, M.L. Doublet, *J. Phys. Chem. C*, 118 (2014) 19023-19031.  
764 [54] J.-S. Filhol, M.-L. Doublet, *Catal. Today*, 202 (2013) 87-97.  
765 [55] J.S. Filhol, M.L. Bocquet, *Chem. Phys. Lett.*, 438 (2007) 203-207.  
766 [56] R.F.W. Bader, *In atoms in Molecules: A Quantum Theory*, Oxford University Press:  
767 Oxford 1990.  
768 [57] J.N. Bronsted, *Chem. Rev.*, 5 (1928) 231-338.  
769 [58] R. P. Bell, *Proc. - R. Soc. London, Sect. A: Math. Phys. Sci*, 1936, 154, 414-429.  
770 [59] M.G. Evans, M. Polanyi, *Trans. Faraday Soc.*, 32 (1936) 1333-1360.  
771 [60] A.L.J. Beckwith, *Chem. Soc. Rev.*, 22 (1993) 143-151.  
772 [61] J.E. Sutton, D.G. Vlachos, *ACS Catal.*, 2 (2012) 1624-1634.  
773 [62] R.A.v. Santen, M. Neurock, S.G. Shetty, *Chem. Rev.*, 110 (2010) 2005-2048.  
774 [63] J.S. McEwen, T. Anggara, W.F. Schneider, V.F. Kispersky, J.T. Miller, W.N. Delgass, F.H.  
775 Ribeiro, *Catal. Today*, 184 (2012) 129-144.  
776 [64] K. Reuter, C. Stampf, M. Scheffler, *AB Initio Atomistic Thermodynamics and Statistical*  
777 *Mechanics of Surface Properties and Functions*, in: S. Yip (Ed.) *Handbook of Materials*  
778 *Modeling*, Springer Netherlands 2005, pp. 149-194.  
779 [65] R.B. Getman, Y. Xu, W.F. Schneider, *J. Phys. Chem. C*, 112 (2008) 9559-9572.  
780 [66] K. Reuter, M. Scheffler, *Phys. Rev. B*, 65 (2001) 035406.  
781 [67] JANAF thermochemical tables, D.R. Stull and H. Prophet, project directors, U.S. Dept. of  
782 Commerce, National Bureau of Standards, Washington, D.C, 1971.  
783 [68] A.L. Dicks, K.D. Pointon, A. Siddle, *J. Power Sources*, 86 (2000) 523-530.  
784 [69] Y. Matsumura, N. Tode, *Phys. Chem. Chem. Phys.*, 3 (2001) 1284-1288.  
785